Characterization of the consequences of Trps1 deficiency in osteoblasts on bone formation

by

Paulina Keskinidis

Bachelor of Liberal Arts, Extension Studies,

Harvard University, 2019

Submitted to the Graduate Faculty of

The University of Pittsburgh School

of Dental Medicine in partial

fulfillment of the requirements for

the degree of

Masters in Oral and Craniofacial

Sciences

University of Pittsburgh

2023

UNIVERSITY OF PITTSBURGH

School of Dental Medicine

This thesis/dissertation was presented by

Paulina Keskinidis

It was defended on April 14, 2023 and approved by

Dr. Konstantinos Verdelis, DDS, PhD, Assistant Professor, Department of Oral and Craniofacial Sciences, Department of Endodontics.

Dr. Guiseppe Intini, DDS, PhD, Associate Professor, Department of Oral and Craniofacial Sciences, Department of Periodontics.

Thesis Advisor: Dr. Dobrawa Napierala, PhD, Associate Professor, Department of Oral and Craniofacial Sciences.

Copyright © by Paulina Keskinidis

2023

Characterization of the consequences of Trps1 deficiency in osteoblasts on bone formation

Paulina Keskinidis, MS

University of Pittsburgh, 2023

TRPS1 is a gene that encodes a zinc-finger transcription factor named TRPS1. Mutations in the *TRPS1* gene cause a rare genetic disease called trichorhinophalangeal syndrome (TRPS), which is inherited in an autosomal dominant manner. Patients with TRPS have a characteristic pear-shaped nose, micrognathia, supernumerary teeth, cone-shaped growth plate in the fingers and toes, delayed bone growth, and osteopenia. To characterize the effect of *Trps1* deficiency in osteoblasts on bone, we analyzed wild-type (WT) and *Trps1*^{Col1a1} conditional knockout (cKO) mice, in which *Trps1* is deleted in osteoblasts upon tamoxifen injection. The WT and *Trps1*^{Col1a1} cKO mice were injected with tamoxifen at postnatal day 1 (P1), P2, P9, P16, and P23. Preliminary analysis of 4-week-old mouse femurs through micro-computed tomography (μCT) suggested that there was less trabecular bone and cortical bone in the *Trps1*^{Col1a1} cKO mice when compared to the WT mice. Hence, we hypothesize that *Trps1* deficiency in osteoblasts impairs bone mass acquisition.

I further analyzed the remaining number of samples needed for our analysis as determined by statistical power analysis to ensure the right sample size for statistical significance (N=5/Genotype/Sex) and found that *Trps1*^{Col1a1} cKO mice had smaller bones. We know that the *Trps1*^{Col1a1} cKO mice have decreased bone mass as indicated by the μCT data. Therefore, we hypothesize that decreased bone mass acquisition is the result of an imbalance in bone homeostasis. In addition to the μCT analysis, my part of the project was to preliminarily determine if there were differences in osteoclasts between the *Trps1*^{Col1a1} cKO and WT mice. To do this, histological analysis was utilized, where distal femur samples were stained with tartrate-resistant acid phosphatase (TRAP) to determine if there were differences in the number of osteoclasts in the *Trps1*^{Col1a1} cKO when compared to the WT mice. Distal femurs N=3 mice/genotype/sex were

sectioned, stained with TRAP, and imaged at 40x magnification. The analysis of the TRAP-stained sections of distal femurs showed no statistical significance of osteoclasts in the trabecular bone and at the chondro-osseus junction in the *Trps1*^{Col1a1} cKO mice in comparison to the WT mice. Quantitative analysis of osteoclasts was conducted utilizing BioQuant software, enabling osteoclast number and surface to be normalized to bone surface.

Table of Contents

Table of Contents

LIST OF FIGURES:

LIST OF TABLES:

1.0 INTRODUCTION

1.1 Brief Overview of *TRPS1*

TRPS1 is a gene that contains 7 exons.[1] In humans, *TRPS1* is located on chromosome 8q23-24 and is 260.5kb long.[2] In both human and mouse, the *TRPS1* gene encodes a GATA-type zinc-finger protein called TRPS1.[2] TRPS1contains nine zinc-finger domains, one of which is a single GATA-type DNA binding domain.[2] Studies have shown that TRPS1 enters the cell nucleus to interact with DNA GATA sequences.[3] Co-transfection experiments demonstrated that TRPS1 acts a transcriptional repressor.[3] In vitro studies have shown that *Trps1* acts as a repressor of five target genes: prostate-specific antigen (KLK3), runt-related transcription factor 2 (RUNX2), signal transducer and activator of transcription 3 (Stat3), parathyroid hormone-related protein (Pthrp), and osteocalcin (BGLAP).[4] TRPS1 also acts as a transcriptional activator, as a study recently showed that Trps1 directly activates Wnt inhibitors Wif1, Apcdd1, and Dkk4, in the vibrissa follicle.[4]

1.2.1.1 Mutations of *TRPS1* Gene

Mutations in the *TRPS1* gene cause a rare disease called trichorhinophalangeal syndrome (TRPS), which is inherited in an autosomal dominant manner. There are three subtypes of TRPS that have been determined. TRPS type I is the result of nonsense mutations, causing haploinsufficiency of *TRPS1*.[5] TRPS type II is caused by contiguous gene deletions that involve *TRPS1* and the neighboring genes *RAD21* and *EXT1*.[5] TRPS type III is the result of missense mutations in exon 6 and 7 of the *TRPS1* gene, which code for the DNA-binding domain, and is the more severe form of TRPS.[5]

Clinical manifestations common to those with TRPS are bulbous tip of the nose, micrognathia, cone-shaped growth plate in the fingers and toes indicated by radiographs, delayed bone growth, osteopenia and, in some cases, osteoporosis.[6] These bone defects in TRPS patients indicate that mutated *TRPS1* disrupts endochondral ossification. TRPS is rare in that it's estimated to affect 1 in every 100,000 people; thus, its prevalence has yet to be fully determined.[7] The reason may be many unreported cases of TRPS, as patients may be undiagnosed because it is hard for clinicians to recognize the physical attributes of TRPS.[8]

1.3 *TRPS1* Role in Endochondral Ossification

There are two processes in which bones are formed, either through intramembranous ossification or endochondral ossification. Bones developed through intramembranous ossification are the cranial bones, clavicle, and flat bones within the face such as alveolar bone.[9] In the process of intramembranous ossification, the mesenchymal cells that originate from the neural crest differentiate into osteoblasts, the cells that secrete osteoid.[9] Mineralization of the osteoid occurs once calcium and phosphate bind to it, at which point the osteoid hardens and becomes bone.[9]

Endochondral ossification is the process of bone formation that begins with a cartilaginous template, which is later replaced by bone. The bones developed via endochondral ossification are the long bones, pelvic bone, and the cranial base. The process begins with mesenchymal cells that originate from the mesoderm, which condensate and differentiate into cells that form cartilage, called chondrocytes.[9] The chondrocytes will proliferate, then they will mature and undergo hypertrophy, and secrete cartilage as the cartilaginous template begins to form.[10] At the outer region of the cartilaginous template is the perichondrium formed by perichondral cells.[11]

Osteoblasts differentiate from mesenchymal cells at the perichondrium to lay down osteoid, and create the bony collar that will become cortical bone, surrounding future trabecular bone within it.[10] Then, the primary ossification center will develop as blood vessels infiltrate the hypertrophic cartilage.[10] The osteoblast progenitors are brought into the hypertrophic cartilage through the blood vessels, which will allow for the osteoblasts to begin the process of bone formation.

Studies have shown that *Trps1* is involved in the process of endochondral ossification, as there is high *Trps1* expression in the regions of mesenchymal condensations where chondrocytes will differentiate from the mesenchymal cells, pre-hypertrophic cells, and perichondral cells.[12] Napierala et al. analyzed the long bones of homozygous $Trps1^{\Delta GT/\Delta GT}$ mice and wild-type (WT)

mice to determine the role of *Trps1* during endochondral ossification.[12-14] *Trps1*$^{\Delta GT/\Delta GT}$ mice showed impaired chondrocyte development when compared to the WT, as there was a delay in hypertrophy of the chondrocytes, suggested by cell morphology and expression of chondrocyte differentiation markers Indian hedgehog (Ihh) and Collagen type X.[12] They also found that the *Trps1*$^{\Delta GT/\Delta GT}$ mice had an increase in mineralized perichondrium when compared to the WT mice, indicating a disruption in the mineralization process.[12] *RUNX2* is a transcription factor that is responsible for chondrocyte hypotrophy and has also been shown to regulate osteoblast differentiation.[12] In addition to the findings in the above mentioned study, Napierala et al. also found that *Trps1* is a repressor of *Runx2* specifically during chondrocyte differentiation and the mineralization of the perichondrium during endochondral ossification.[12]

TRPS1 has been shown to repress Plasminogen activator inhibitor 2 (*SerpinB2*), which is upregulated by inorganic phosphate (P_i) specifically when mineralization begins in committed osteogenic cell lines.[15] Socorro et al. utilized *Trps1*-deficient, *Trps1*-overexpressing, and 17IIA11 (control) cell lines to analyze the effects of *Trps1* on *SerpinB2*.[15] The mRNA levels of *SerpinB2* showed the overexpression of Trps1 decreased the expression of P_i-stimulated *SerpinB2*.[15] Overall, Socorro et al. found that *SerpinB2* is downregulated by Trps1, an increase in *Trps1* hinders the upregulation of *SerpinB2*, and *SerpinB2* deficiency causes impaired and decreased mineralization in committed osteogenic cell lines.[15] Therefore, *Trps1* deficiency in cells that form mineralized ECM impairs their mineralization ability.

1.4 Bone Remodeling

Our bones constantly undergo bone remodeling for repair of microfractures that are caused by daily activities, rearranging bone structure for enabling mechanical load, and for preserving systemic calcium homeostasis.[16] The two types of cells that are imperative to bone remodeling are osteoclasts and osteoblasts. Bone remodeling is initiated by the osteoclasts that resorb bone, and then followed by the osteoblasts which build bone.

The tightly coupled communication between osteoclasts and osteoblasts ensures that there is not too much resorption by osteoclasts and not enough bone formed by the osteoblasts.[17] However, age, medications, or genetic mutations may cause an imbalance in this process, resulting in the resorption of bone to surpass the amount of bone formed.[17] This leads to excessive bone loss, causing lower bone mass, and ultimately, bone fragility, as is seen in cases of osteopenia and osteoporosis—common clinical characteristics of TRPS patients.

1.5 Osteoclasts and Osteoblasts

Osteoblasts form bone as they secrete osteoid, which is unmineralized extracellular matrix consisting of collagen and proteoglycans.[9] Calcium phosphate crystals then binds to the osteoid, leading to its mineralization, and ultimately becoming bone.[9] Osteoblasts are not only responsible for forming bone, but also play a role in bone homeostasis through tightly coupled communication with osteoclasts. There are various pathways in which osteoclasts and osteoblasts communicate such as, the OPG/RANKL/RANK, LGR4/RANKL/RANK, Ephrin/ephB4, Sema3A/Nrp, and MSF/MCP-1 pathways.[18] However, the predominant pathway that regulates osteoclast differentiation is the OPG/RANKL/RANK pathway. Osteoblasts secrete osteoprotegrin (OPG), which act as a decoy receptor, binding to receptor activator of NF-κB ligand (RANKL) and preventing RANKL binding to receptor activator of NF-κB (RANK).[19] Osteoblasts also secrete RANKL, which binds to RANK, activating the osteoclast differentiation process.

Osteoclasts are multinucleated cells that are differentiated from monocyte macrophages.[20] Osteoclasts actively resorb bone when they are considered mature osteoclasts, which occurs when the osteoclast mononucleated precursors become polarized and fuse together with other osteoclast precursors to become multinucleated osteoclasts once RANKL binds to RANK.[19] Mature osteoclasts will attach to the surface of the bone forming a ruffle border, where the osteoclasts will release enzymes cathepsin-K and hydrochloric acid to degrade the bone.[19]

1.6 Mouse Model

It has been shown that patients with TRPS tend to suffer from osteopenia and in some cases, osteoporosis. As mentioned earlier, the microarchitecture of bone is important for withstanding mechanical forces and those with low bone mass are more prone to fractures. To investigate this, our lab generated *Trps1*^{col1a1} conditional knockout (cKO) mice, in which *Trps1* is specifically deleted in odontoblasts and osteoblasts upon tamoxifen injection. For the purposes of my project, I will focus on discussing the conditional deletions in the osteoblasts. The reason why we did not utilize knock-out mice is because the literature has shown that *Trps1*$^{-/-}$ mice die neonatally due to respiratory failure.[13] In addition, *Trps1*$^{-/-}$ have been shown to have severe effects from the *Trps1* mutation such as cleft palate, while *Trps1*$^{+/-}$ mice exhibit similar manifestations of TRPS to those seen in humans with TRPS.[21] However, utilizing a conditional mouse model enables us to knock-out *Trps1* specifically in osteoblasts and analyze mouse bone, postnatally. Therefore, we generated this *Trps1*^{col1a1} cKO model to delete *Trps1* specifically in osteoblasts for determining its effects on bone mass acquisition.

The way in which the *Trps1*^{col1a1} cKO mice were generated was through utilization of the Cre-*lox* system. The Trps1 gene was deleted in osteoblasts through a tamoxifen inducible Cre recombinase via the *2.3kbCol1a1-Cre*^{ERT2} driver, JAX stock #016241.[22] The Cre protein is restricted to the cytoplasm, so it can only enter the nuclear compartment after tamoxifen injections.[22] Through this method, fifty percent of the offspring are *Trps1*^{col1a1} cKO and the remaining fifty percent are wild-type controls (WT).

Both WT and *Trps1*^{col1a1} cKO mice were injected with 0.1 mg/g of tamoxifen at postnatal day 1 (P1), P2, P9, P16, and P23. The WT mice were injected in addition to the *Trps1*^{col1a1} cKO mice to reduce experimental variables, because studies have shown that tamoxifen can increase

bone mineral density in mice as it has estrogen-like effects on bone.[23] Tail tips were collected first at day 9 and then again at 4 weeks, when the mice were sacrificed. The tail tips were used for genotyping by polymerase chain reaction (PCR), to ensure that the Cre was expressed. We analyzed mice at 4-week of age, because this is the stage of dynamic bone formation and remodeling (as an adaptation to growth), hence osteoblasts and osteoclasts are highly active at this age. From a histological standpoint, it is also a good age to analyze the various stages of chondrocyte differentiation in the femur as the bone is actively growing.

3.0 SPECIFIC AIMS AND HYPOTHESIS

A common clinical characteristic of TRPS is osteopenia, and sometimes the more progressed form, osteoporosis. Additionally, it has been shown through a genome-wide association study that *TRPS1* is associated with low bone mineral density.[24] Studies from our lab have shown that *Trps1* plays a role in the development of endochondral bones and bones within the craniofacial region such as the jaw.[10] It has been shown that *Trps1* deficient mice have impaired chondrocyte differentiation and premature mineralization of the perichondrium. Studies have also shown that *Trps1* represses *Runx2* during endochondral ossification.[12] In addition, in vitro studies show *Trps1* deficiency in cells that form mineralized extracellular matrix (ECM) impairs their mineralization ability.[15]

We generated a conditional knockout mouse model where *Trps1* is specifically deleted in osteoblasts upon tamoxifen injections, to evaluate the role of *Trps1* deficiency in osteoblasts on bone development. Preliminary data from our lab suggested that there is a decrease in trabecular thickness in mice with *Trps1* deficiency in osteoblasts shown by quantitative and 3D μCT renderings of the distal femurs and alveolar bone of 4-week-old mice. Preliminary data of Tartrate-Resistant Acid Phosphatase (TRAP) staining of alveolar bone also suggested differences in osteoclasts between the mice with *Trps1* deficiency in osteoblasts when compared to the wild-type mice.

We analyzed the distal femurs of the wild-type (WT) and $Trps1^{Col1a1}$ cKO mice. The following aims below serve to address if our model of *Trps1* deficiency in osteoblasts impairs bone mass acquisition and determine the mechanism causing low bone mass in our mouse model. We hypothesize that *Trps1* deficiency in osteoblasts causes decreased bone mass in TRPS patients. The following aims were used to test our hypothesis.

Aim 1: Determine if *Trps1* deficiency in osteoblasts has an effect on bone microarchitecture and size in the distal femurs and alveolar bone. To test this, we utilized μCT scans to analyze and compare bone microarchitecture between the WT and the *Trps1*^{col1a1} cKO mice for males and females to determine if there are any differences. Preliminary data has shown that there is a decrease in trabecular thickness in the *Trps1*^{col1a1} cKO femurs and alveolar bone. We hypothesize that the *Trps1*^{col1a1} cKO mice will have less bone mass due to *Trps1* deficiency in the osteoblasts.

Aim 2: Determine if *Trps1* deficiency in osteoblasts has an effect on osteoclasts. To test this, we stained distal femurs of 4-week-old male and females, *Trps1*^{col1a1} cKO and WT mice, with TRAP as a marker for osteoclasts. We then utilized BioQuant OSTEO software for quantification of osteoclasts to determine osteoclast surface normalized to bone surface and osteoclast number normalized to bone surface. We know that *TRPS1* is a repressor of *RUNX2* which is a regulator for osteoblast differentiation and GWAS have associated *TRPS1* with low bone mineral density. We hypothesize that the *Trps1*^{col1a1} cKO mice will have a disruption in bone homeostasis, so we must identify if there are differences in osteoclast numbers. We hypothesize that the low bone mass in the *Trps1*^{col1a1} cKO mice is a result of more osteoclasts when compared to the osteoclast number in the WT mice.

4.0 MATERIALS AND METHODS

4.1 Statistical Analysis

For the quantitative analysis of the μCT data, and the osteoclast number/surface per bone surface, the values of each of the parameters analyzed were exported into a Microsoft Excel file and were analyzed by pasting the values into Graph Pad Prism 9.0. For the statistical analysis comparing the values between the *Trps1*^{col1a1} cKO and WT mice in both males and females, the unpaired t-test was used where statistical significance was indicated by the following: *-$p \leq 0.05$, **$p \leq 0.01$, *** $p \leq 0.001$, and **** $p \leq 0.0001$. The graphs for each parameter were then created using Graph Pad Prism 9.0.

4.2 Mouse Femur Sample Preparation

The analyses were conducted on formalin-fixed left hindlimbs and left half heads that were previously harvested from WT and *Trps1*^{Col1a1} cKO mice. The tissues were previously fixed in formalin for 24 hours, then rinsed in PBS and stored in 70% ethanol for µCT analysis. The paraffin embedded left hindlimbs were sectioned 7µm in thickness using a microtome (Figure 1). The maintenance and euthanizing of the mice used in these experiments followed the regulations and guidelines approved by the Institutional Animal Care and Usage Committee (IACUC) and those set forth in our mouse protocols.

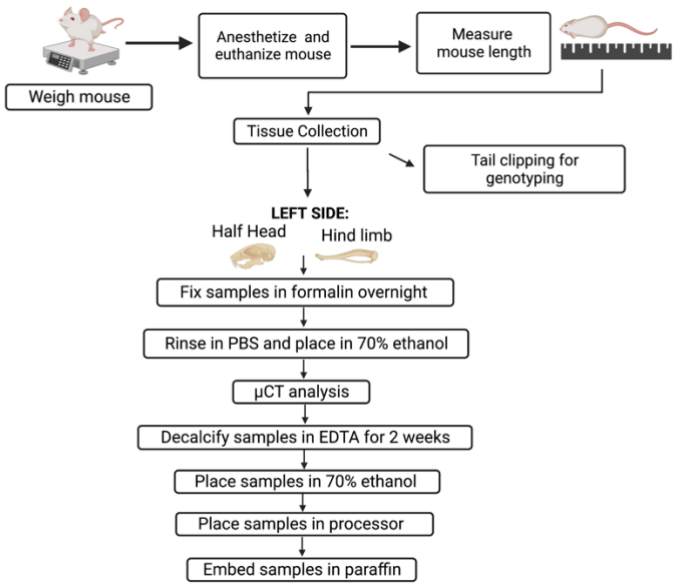

Figure 1: Schematic of tissue collection and processing of samples. The schematic illustrates the process in which the mice were euthanized, and the samples were collected and stored for micro-computed tomography and histological analysis. Created with Biorender.com

4.3 Microcomputed Tomography (μCT) Studies

The left distal femurs and left half head of 4-week-old WT (n=5/sex) and *Trps1*^{Col1a1} cKO (n=5/sex) mice were collected and placed in 70% ethanol (EtOH) for microcomputed tomography (μCT) analysis. We utilized the Scanco μCT 50 (Scanco Medical, Brüttisellen, Switzerland) software to evaluate the microarchitecture of the trabecular and cortical bone in the femurs and trabecular bone in the alveolar bone to compare between the WT and *Trps1*^{Col1a1} cKO mice. The samples were all scanned at 6 μm voxel size.

The way in which the trabecular bone was analyzed through μCT is that the file containing the 2D images of the scans conducted by Lydumila Lukashova were opened and zoomed 4x on the desired sample indicated by the scanning processing sheet. Then, the threshold was chosen by opening the "contours" window and looking at the grayscale. The greyscale was previewed and adjusted. The threshold was then lowered until both the greyscale and threshold were at the same parameters. Then, the start points of contouring the trabecular bone was selected by scrolling through the slices past the growth plate until the "+ shape" of the growth plate was no longer visible. From that point, 10 slices were added to determine the start point (Figure 2, A). The contours were then drawn, and the end point was 200 slices from the starting point for all the samples (Figure 2, B). The threshold of all samples was set to 280 for the trabecular bone of the femur.

For the cortical bone μCT analysis, the threshold was chosen by opening the "contours" window and looking at the grayscale. The greyscale was previewed and adjusted. The threshold was then lowered until both the greyscale and threshold were at the same parameters. The threshold for the cortical bone was 390 for all the analyzed samples. The start point was the slice where the 2D image of the trabecular bone was no longer visible (Figure 2, C). The contours of the outer bone

were drawn in a counterclockwise direction for the “single” contours. Next, the “double” contours were drawn on the inside of the cortical bone in a clockwise direction to exclude the bone marrow (Figure 2, C and D). The finish point of cortical bone was the point where 150 slices were subtracted from the starting point (Figure 2, D).

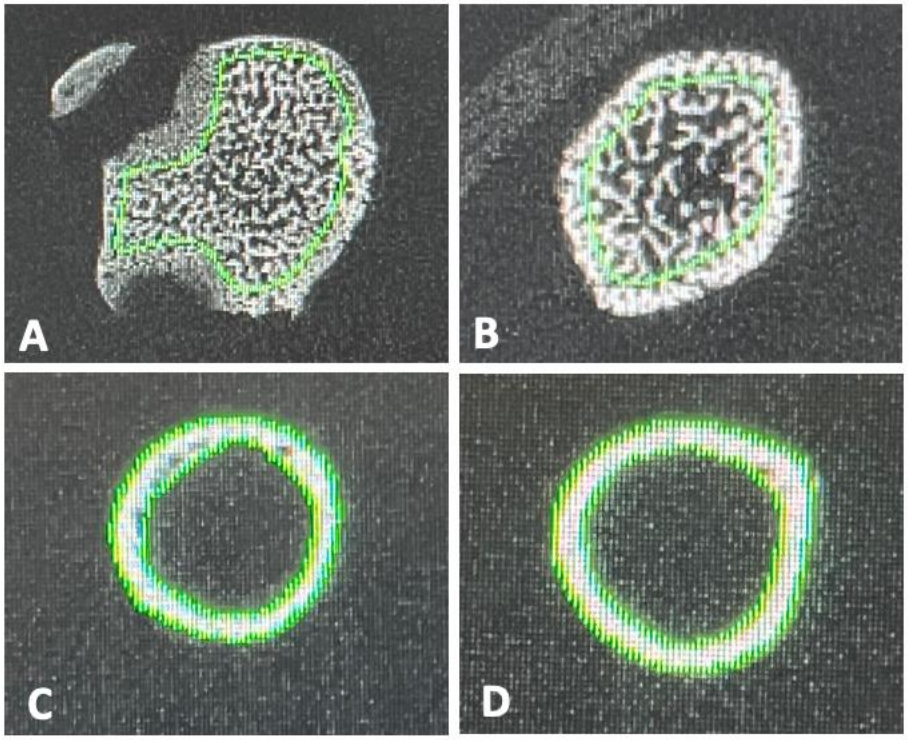

Figure 2: Images of start and end point of trabecular bone (A and B) and cortical bone (C and D) analysis. A shows the start point of the trabecular bone analysis and B is the end point. C is the start point of the cortical bone analysis and D is the end point.

For the alveolar bone analysis, the slice of the first molar was chosen where the incisor was not visible. Then, the start point was selected by scrolling through the slices until the 3rd molar was visible (Figure 3, A). The end point was the point at which the molar was no longer visible (Figure 3, B). The “upper threshold” was set to 1000 for all the samples. Once this file was analyzed by the software, it created an “aim” file, which was then opened in 3D for the cusps of the molars to be facing upward for further analysis (Figure, 4).

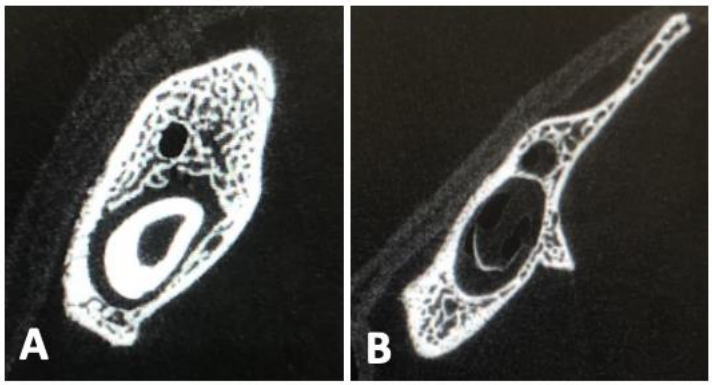

Figure 3: Images of start and end point of alveolar bone analysis (A and B). A shows the start point of the alveolar bone analysis and B is the end point.

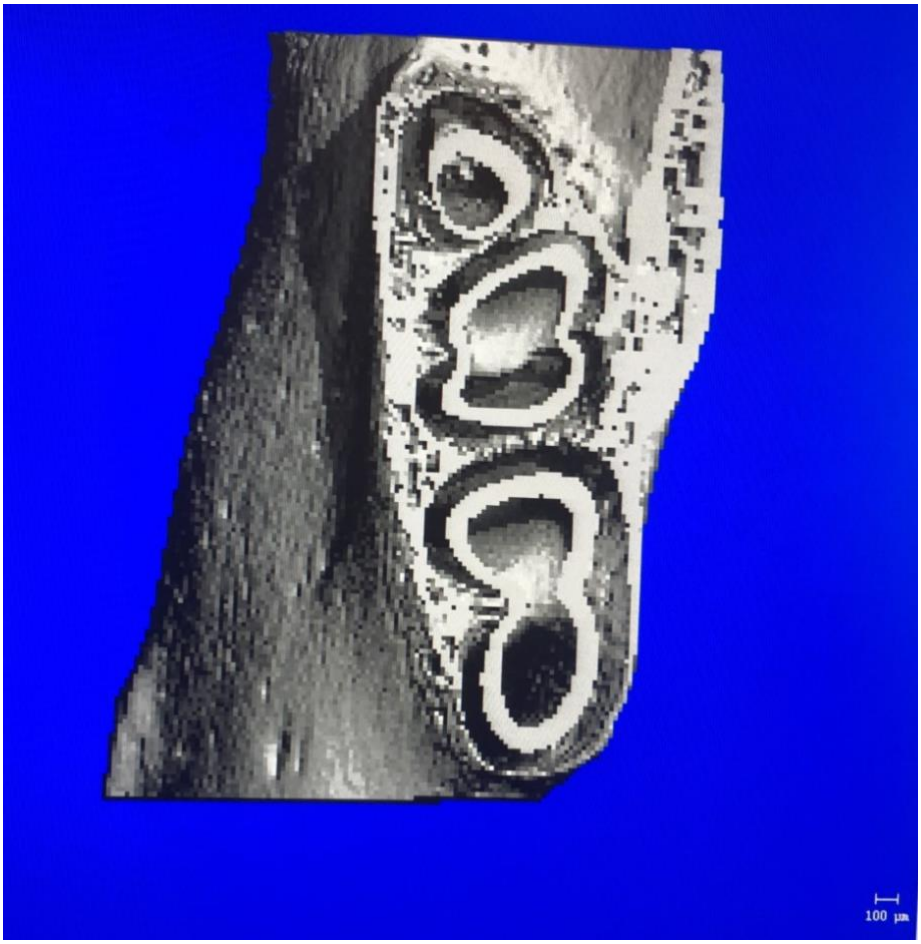

Figure 4: 3D image of alveolar bone with molars facing upward.

The new file was created where the image was rotated and there was a clear view of the alveolar bone with the molars facing upward. The next step was to contour the alveolar bone in a

counterclockwise direction. Then the roots of the 1st and 2nd molar, were contoured in a clockwise direction to exclude the molars so that the alveolar bone could solely be analyzed (Figure 5).

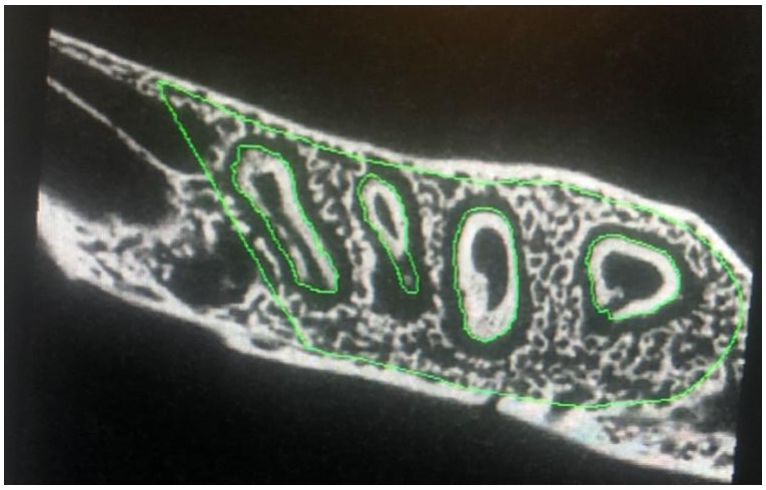

Figure 5: 2D image of alveolar bone. This image shows the alveolar bone contours and the contours of the molars. The molars were excluded, and the alveolar bone was solely analyzed.

4.4 Histological Studies

The slices of the paraffin embedded hindlimbs were placed on the slides in a series manner, where three tissue sections collected from regions approximately 50 microns apart were placed onto one slide. The first section was placed in a slide labeled 1-1, then the second one was placed on a slide labeled 2-1, and so forth. This series technique was utilized to ensure we analyzed the 3D tissue samples at different depths.

The slides were then placed on a heat block overnight for the samples to dry onto the slides. The sample slides were deparaffinized and rehydrated prior to the TRAP staining. They were placed in xylene twice for 3 minutes each time, then in 100% ethanol twice for 3 minutes each time. Then, the samples were placed twice for 1 minute in 95% ethanol, and after, in 70% ethanol once for 1 minute. The samples were then placed in deionized water for one minute. The 0.2M acetate buffer was made using 50mL of deionized water, 0.2M of sodium acetate (Thermo Fisher catalog number: AAA1318430), and 0.077M of L(+) tartaric acid (Sigma catalog number: 251380). The solution was placed on a stir plate with a magnetic stir bar inside of it. The buffer needed to be at a pH of 5.0, so NaOH was added until the pH was 5.0.

The deparaffinized and rehydrated slides were removed from the deionized water and were placed in the 0.2M acetate buffer for 20 minutes at room temperature. After the 20 minutes, 0.0013M of naphthol-AS-MX-phosphatase (CAS No. 1596-56-1. Lot 154161-173992) and 0.0085M of fast red TR salt hemi (zinc chloride) salt (Sigma Aldrich catalog number: 368881-25G) were added to the 0.2M Acetate buffer. The slides were incubated for 30 minutes at 37^{o} C and rinsed under running tap water for 1 minute (Figure 6, A). The samples were each covered with a drop of Immu-Mount™ (Thermo Scientific), covered with a coverslip and let to sit overnight to ensure proper drying.

The samples were then imaged at 40x magnification at three regions as shown on Figure 6, the chondro-osseous junction (region A) and the trabecular bone (region B and C). The trabecular bone analysis contained both B and C regions to ensure a more representative analysis of the trabecular bone, rather than looking at one region. The images taken were set at an exposure time of 3.2 ms.

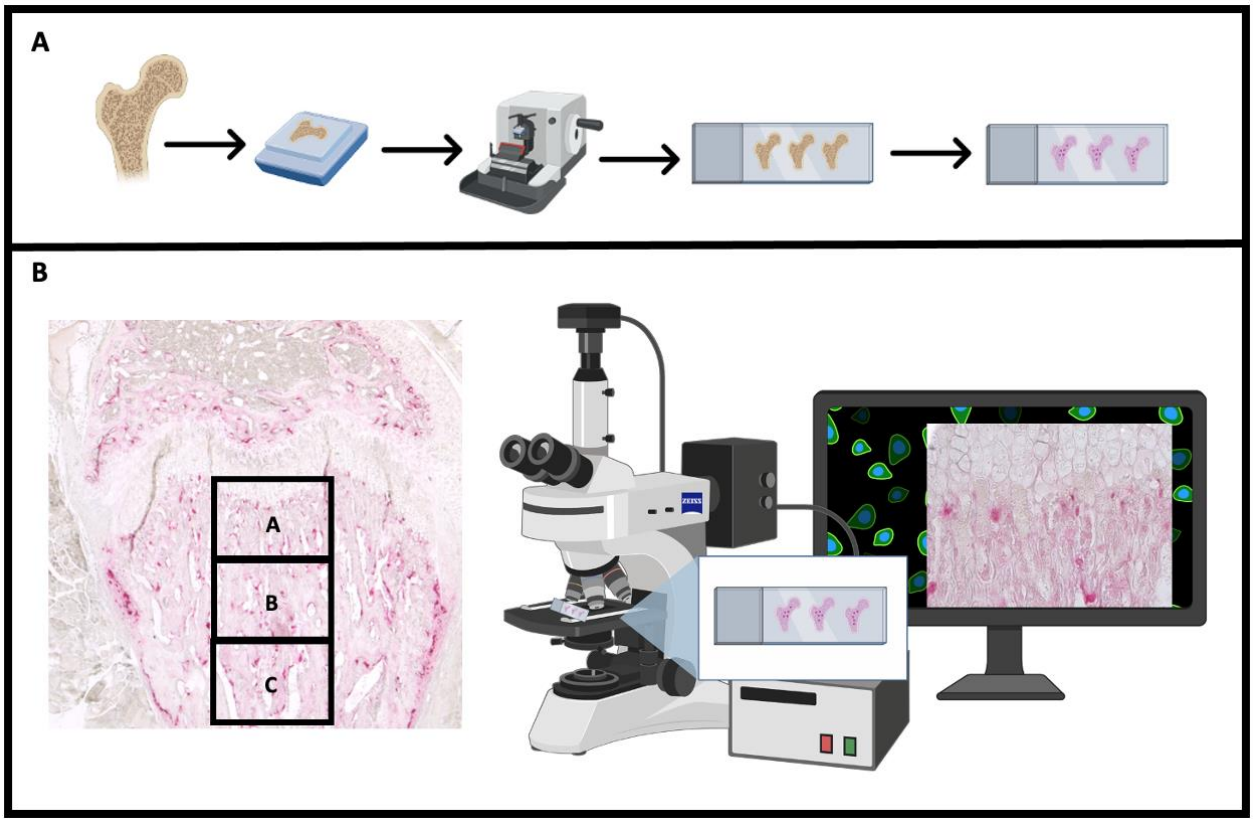

Figure 6: Schematic illustrating the osteoclast analysis. Figure A: the process of the femur isolation, showing that the samples were sectioned, mounted on slides, and stained for detection of Tartrate-Resistant Acid Phosphatase (TRAP). Figure B: the analysis was done at the chondro-osseous junction (region A), and at the trabecular bone (region B and C). Image created with Biorender.com.

4.5 Osteoclast Quantitative Analysis

The 40x images of the TRAP-stained femurs were analyzed using BioQuant OSTEO software. The osteoclast analysis at the chondro-osseous region was conducted separately than the trabecular bone because there is a mixture of cartilage at the chondro-osseous junction. Thus, it would not be accurate to count this region as trabecular bone. The osteoclasts resorb cartilage in the chondro-osseous junction during endochondral ossification. Therefore, the chondro-osseous junction was analyzed as one of the regions for the osteoclast analysis. The first step of the chondro-osseous junction analysis was to select the regions that appeared to be cartilage, which was a lighter pink color and was easy to distinguish between the marrow. Then, the darkly stained osteoclasts that were on the surface of the selected cartilage were selected by drawing the surface that the osteoclasts were resorbing.

The trabecular bone region was analyzed because trabecular bone is important for maintaining the structure of bone and the osteoclasts are particularly active in this region as they are repairing microfractures from mechanical load. The trabecular bone analysis was done in a similar manner as the chondro-osseous junction, as the bone regions were first selected and measured. Then, the osteoclasts were selected by selecting the larger, darkly stained pink osteoclasts that were on top of the selected trabecular bone because osteoclasts resorb the surface of the bone. Thus, only the osteoclasts that appeared to be on the surface of the bone were selected.

5.0 RESULTS

5.1 µCT Analysis of *Trps1*^{Col1a1} cKO Mice versus WT Mice

The µCT analysis was utilized to investigate the role of *Trps1* in bone through its deficiency in osteoblasts. To do this, we analyzed the quantity, microarchitecture, and mineralization of the trabecular bone and cortical bone in 4-week-old left distal femurs of male and female WT (n=5/sex) and *Trps1*^{col1a1} cKO (n=5/sex). We also looked at the trabecular bone of the alveolar bone from the left head of male and female WT (n=5/sex) and *Trps1*^{col1a1} cKO (n=5/sex) mice. The values for both male and female WT and *Trps1*^{col1a1} cKO mice were analyzed. For the trabecular bone of the femurs and alveolar bone, the parameters evaluated were: total volume (TV), bone volume (BV), bone volume fraction (BV/TV), trabecular thickness (Tb.Th), tissue mineral density (TMD), trabecular number (Tb.N), connectivity density (Conn.D), trabecular separation (Tb.Sp), and specific bone surface (BS/BV). The parameters analyzed for trabecular bone of the alveolar bones were: TV, BV, BV/TV, Tb.N, Conn.D, and TMD. For the cortical bone analysis, the parameters evaluated were, TMD, TV, BV, BV/TV, cortical porosity (Ct.Po), and cortical thickness (Ct.Th) for male and female WT and *Trps1*^{col1a1} cKO mice.

The trabecular bone analysis revealed significant differences. There was decreased total volume, bone volume, and bone volume fraction in the *Trps1*^{col1a1} cKO females (Figure 7), indicating that the *Trps1*^{col1a1} cKO females have less trabecular bone contribution to the femurs and that they have smaller bones in comparison to the WT females. Similar to the *Trps1*^{col1a1} cKO females, the *Trps1*^{col1a1} cKO males had decreased bone volume, indicating less trabecular bone in the femurs. However, the *Trps1*^{col1a1} cKO males did not have any statistically significant differences in total volume or bone volume fraction (Figure 7).

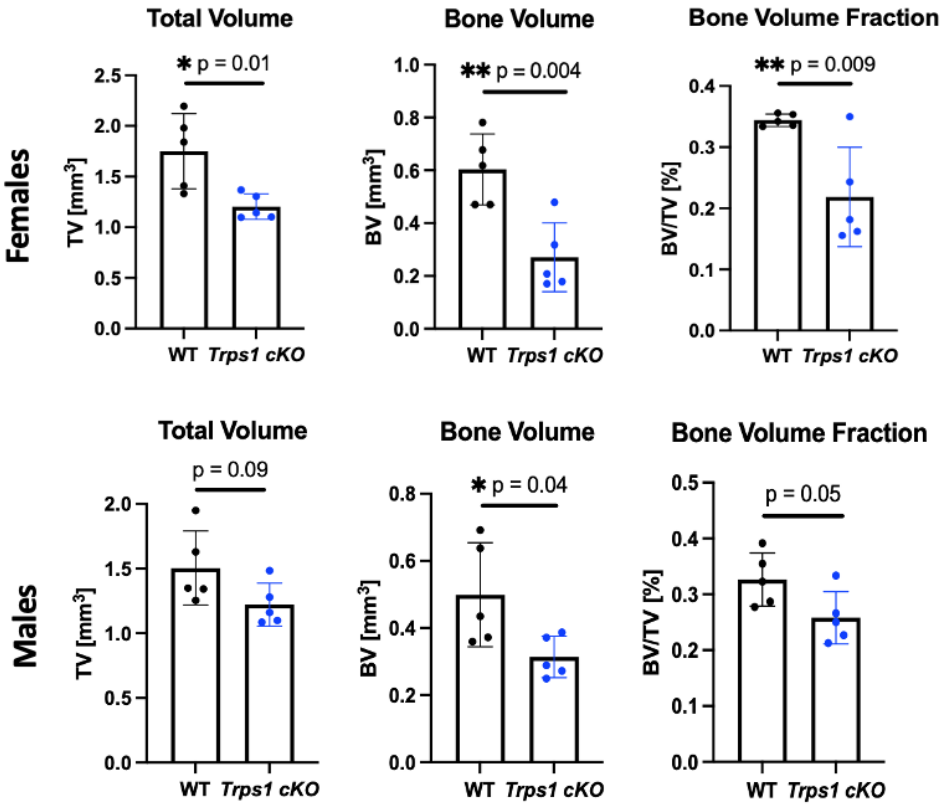

Figure 7: Comparison of total volume, bone volume, and bone volume fraction of trabecular bone in distal femur of WT and *Trps1*^{col1a1} cKO females and males. There is decreased TV, BV, and BV/TV in the *Trps1*^{col1a1} cKO females. There is decreased BV in *Trps1*^{col1a1} cKO males. The difference is not statistically significant in TV or BV/TV in the *Trps1*^{col1a1} cKO males when compared to WT males. Statistical significance is indicated by the asterisks beside the p-values: *-$p \leq 0.05$, **$p \leq 0.01$.

The representative 3D renderings in Figure 8 show the comparison of thickness between the WT and *Trps1*^{col1a1} cKO. The color map shows the thickness ranging from 0.000mm to 0.090mm. The WT shows to have thicker trabecular bone when compared to the *Trps1*^{col1a1} cKO. There was less trabecular bone formed in the *Trps1*^{col1a1} cKO male and female mice, as the results of the quantitative analysis indicate there is decreased trabecular thickness in the male and female *Trps1*^{col1a1} cKO mice when compared to the WT (Figure 9).

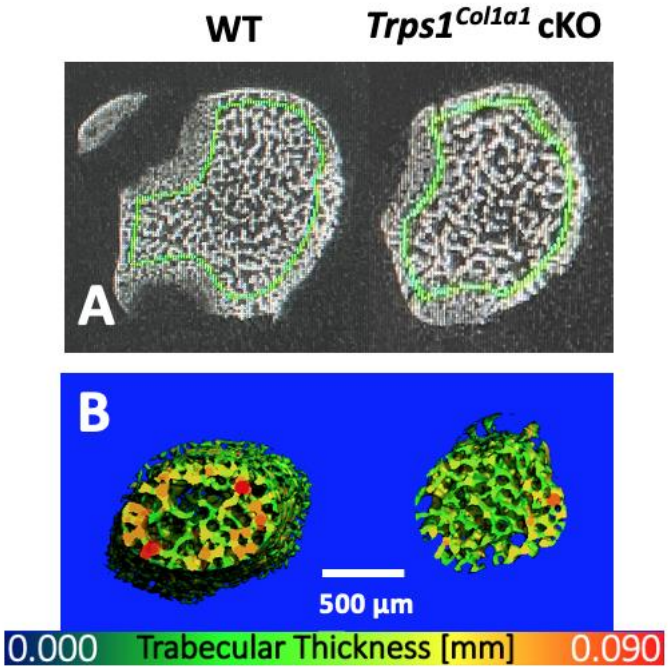

Figure 8: 2D and 3D renderings of the trabecular bone. Figure A shows the 2D images of the comparison of the WT and *Trps1*^{col1a1} cKO mice. Figure B shows the color map of the trabecular bone comparison of the WT and *Trps1*^{col1a1} cKO mice. The trabecular thickness is indicated ranging from 0.000 to 0.090, where the red regions indicate thicker trabecular bone. These 3D images were rendered by Priyanka Hoskere.

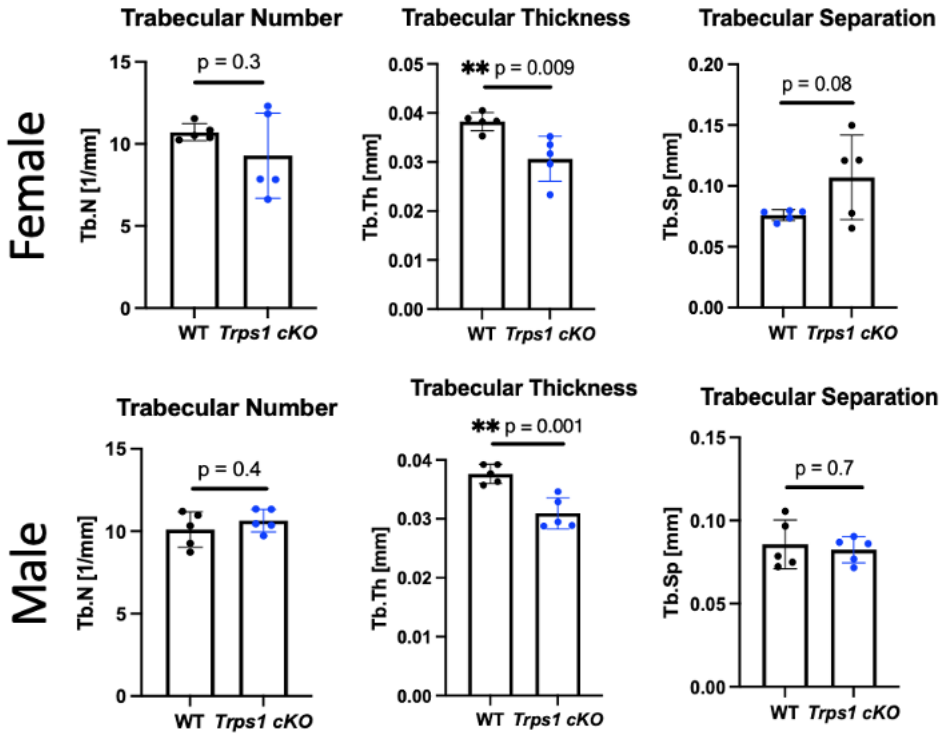

Figure 9: Comparison of WT and *Trps1*^{col1a1} cKO males and females trabecular number, trabecular thickness, and

trabecular separation. There is no statistical significance in Tb.N or Tb.Sp in males and females. There is decreased trabecular thickness in *Trps1*^{col1a1} cKO male and females. Statistical significance is indicated by the asterisks beside the p-values: **$p \leq 0.01$.

There was no statistical significance in the trabecular number or trabecular separation in the WT and *Trps1*^{col1a1} cKO females and males (Figure 9). There were no significant differences in connectivity density in the WT and *Trps1*^{col1a1} cKO females and males (Figure 10). There is increased specific bone surface in the *Trps1*^{col1a1} cKO females and males when compared to the WT (Figure 11). Specific Bone Surface is defined as the "total internal surface area per unit volume of bone tissue."[25] Thus, our results indicate the increase in bone surface is the result of uneven trabecular bone in the *Trps1*^{col1a1} cKO mice when compared to the WT. The literature has also stated that higher specific bone surface indicates increased bone remodeling.[25] Thus, our results infer an increase in bone remodeling in the *Trps1*^{col1a1} cKO males and females when compared to the WT.

The μCT analysis detected the *Trps1*^{col1a1} cKO females have decreased tissue mineral density when compared to the WT females, but the males do not have any statistical significance. However, the quantitative analysis (Figure 12) shows the values to be very close between the WT and *Trps1*^{col1a1} cKO in both sexes, with significance in females but not the males. This could suggest that even though there is statistical significance in the females, it is minimal and may mean that the mineralization is not affected biologically.

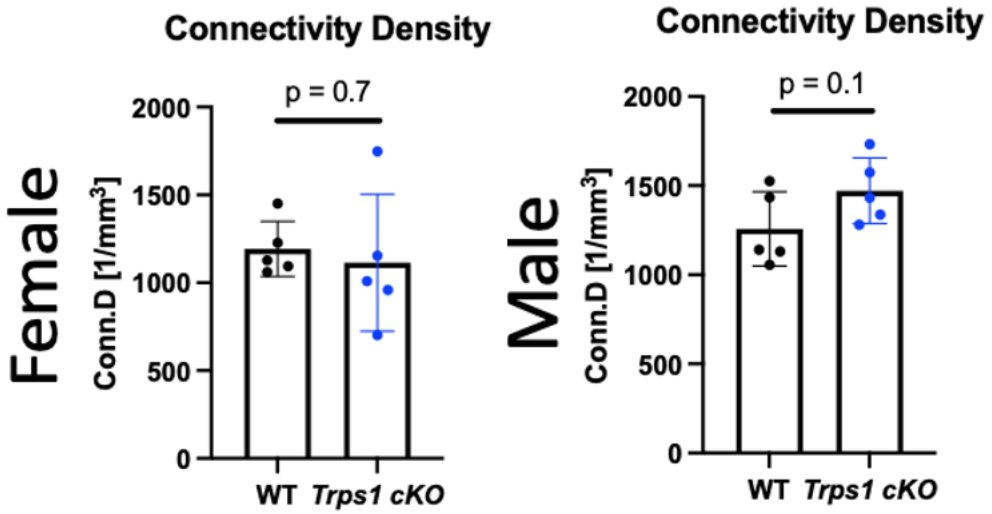

Figure 10: Comparison of connectivity density for WT and *Trps1*^{col1a1} cKO males and females of trabecular bone. There is no statistical significance.

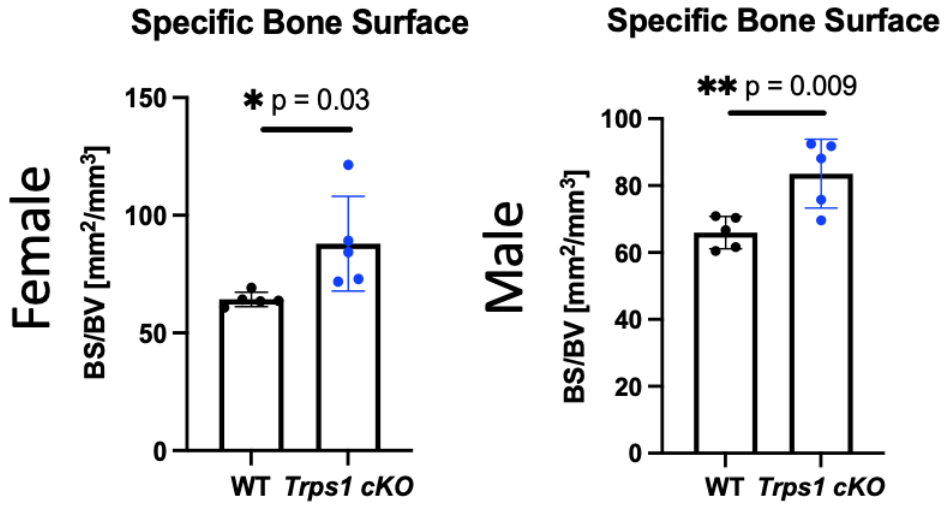

Figure 9: Comparison of WT and *Trps1*^{col1a1} cKO males and females specific bone surface. There is increased specific bone surface in *Trps1*^{col1a1} cKO females and males. Statistical significance is indicated by the asterisks beside the p-values: *-p ≤ 0.05, **p ≤ 0.01.

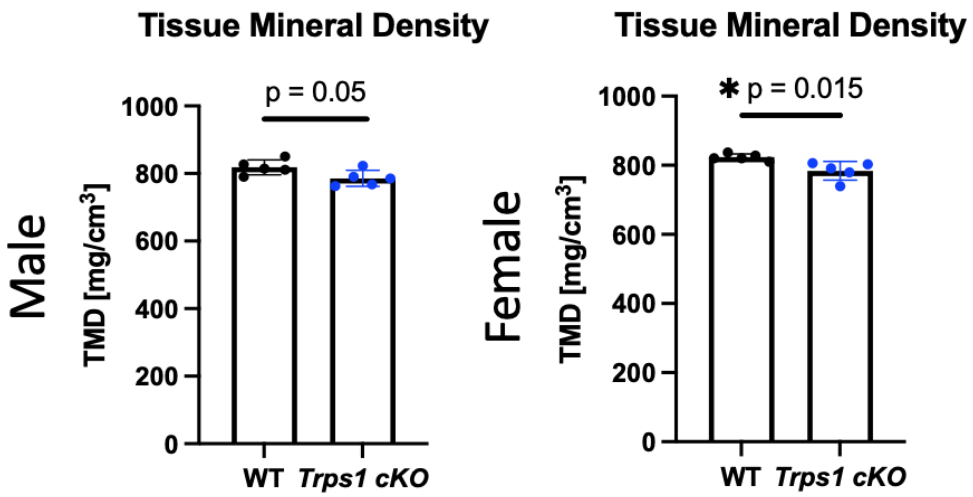

Figure 10: Comparison of WT and *Trps1*^{col1a1} cKO male and female tissue mineral density of trabecular bone. There is decreased tissue mineral density in *Trps1*^{col1a1} cKO females. No statistical significance in males. Statistical significance is indicated by the asterisks beside the p-values: *-p ≤ 0.05.

For the cortical bone analysis, the *Trps1*^{col1a1} cKO females had decreased total volume, bone volume, and bone volume fraction (Figure 13). These results indicate that the *Trps1*^{col1a1} cKO females had less cortical bone, and in correlation to the trabecular bone analysis, further confirming that the femurs are smaller in the *Trps1*^{col1a1} cKO females compared to the WT females. The *Trps1*^{col1a1} cKO females showed an increase in Cortical Porosity (Figure 13), meaning the cortical bone is more porous and therefore more susceptible to fractures due to the compromised bone quality.

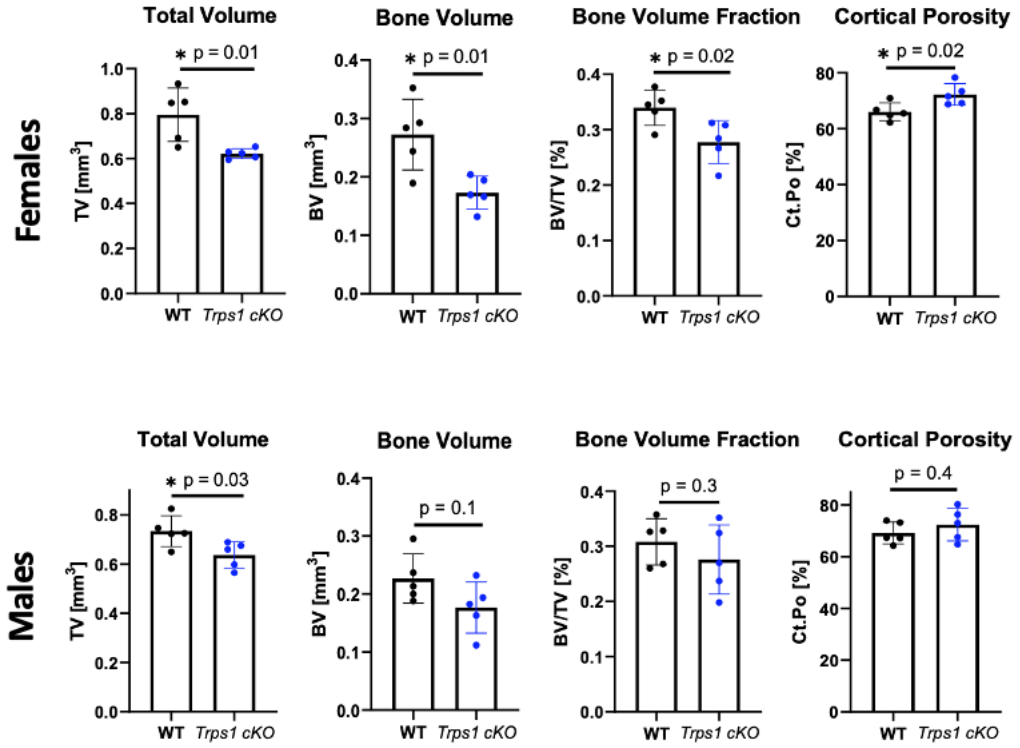

Figure 11: Comparison of WT and *Trps1*^{col1a1} cKO total volume, bone volume, bone volume fraction, and cortical porosity for females and males. There is decreased TV, BV, BV/TV in *Trps1*^{col1a1} cKO females. There is an increase in Ct.Po in *Trps1*^{col1a1} cKO females. There is decreased TV in *Trps1*^{col1a1} cKO males but no statistical differences in BV, BV/TV, or Ct.Po in *Trps1*^{col1a1} cKO. Statistical significance is indicated by the asterisks beside the p-values: *-p ≤ 0.05.

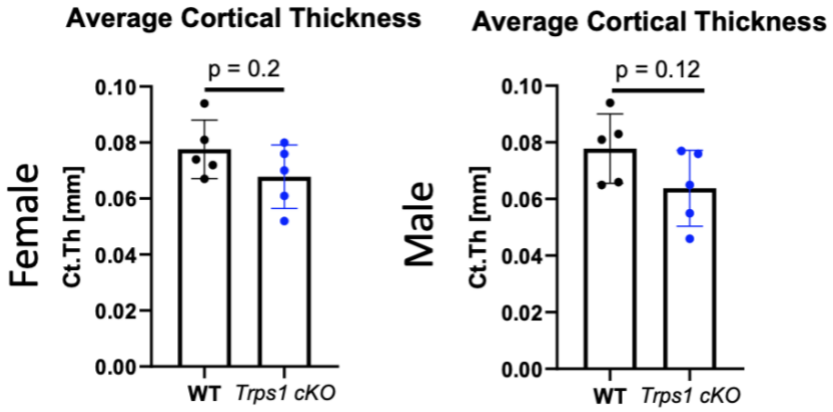

Figure 12: Comparison of WT and *Trps1*^{col1a1} cKO males and females average cortical thickness. There is no statistical significance.

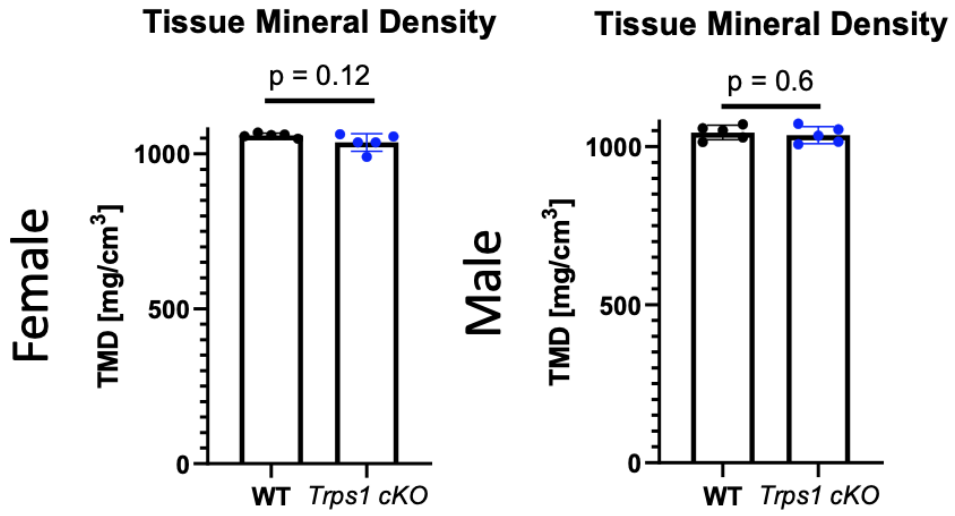

Figure 13: Comparison of WT and *Trps1*^{col1a1} cKO male and female tissue mineral density of cortical bone. There is no statistical significance.

Similar to the quantitative analysis of the female cortical bone investigating total volume, the *Trps1*^{col1a1} cKO males showed to have decreased total volume indicating less cortical bone when compared to the WT males. However, there were no significant differences in the bone volume, bone volume fraction, or cortical porosity (Figure 13). There were no significant differences in the average cortical thickness in either males or females, indicating there is no effect on cortical thickness (Figure 14). The Tissue Mineral Density analyses in the cortical bone did not show any statistical significance between the *Trps1*^{col1a1} cKO and WT females and males (Figure 15). Therefore, the cortical bone did not have impaired mineralization.

The *Trps1*^{col1a1} cKO females and males showed decreased total volume, bone volume, and bone volume fraction in the trabecular bone of the alveolar bone (Figure 16). These results tell us that there is decreased trabecular bone, decreased trabecular bone contribution to the alveolar bone, and smaller alveolar bones in the *Trps1*^{col1a1} cKO females and males when compared to the WT females and males.

There is a decrease in Trabecular Number and Connectivity Density in the *Trps1*^{col1a1} cKO

when compared to the WT mice in both females and males (Figure 17). This indicates smaller and potentially more fragile alveolar bone.

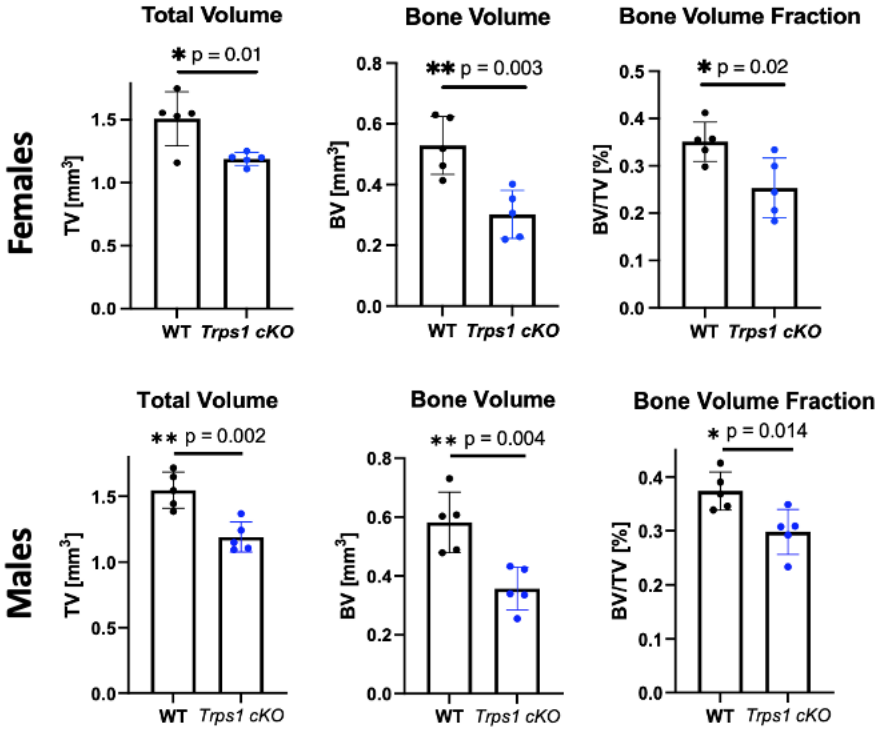

Figure 14: Comparison of WT and *Trps1*^{col1a1} cKO female and male total volume, bone volume, and bone volume fraction in the alveolar bone. There is decreased TV, BV, BV/TV in the *Trps1*^{col1a1} cKO females and males when compared to the WT. Statistical significance is indicated by the asterisks beside the p-values: *-$p \leq 0.05$, **$p \leq 0.01$.

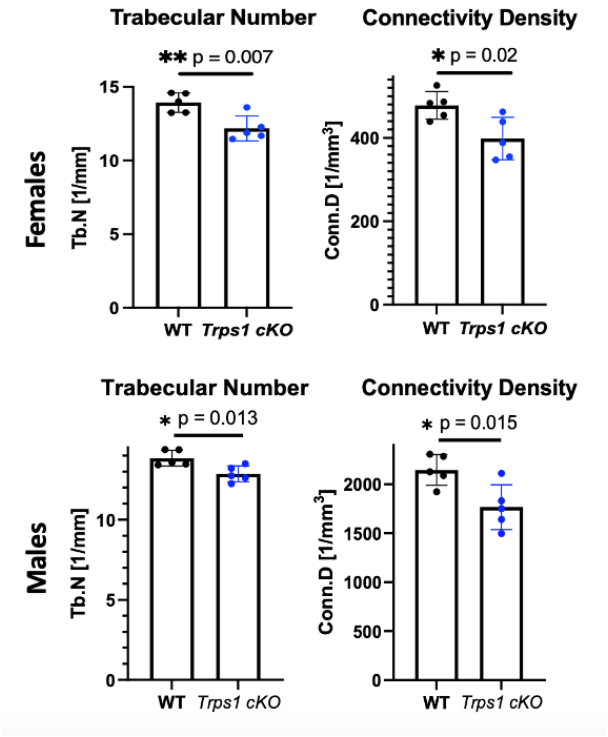

Figure 15: Comparison of WT and *Trps1*^{col1a1} cKO female and male trabecular number and connectivity density in the alveolar bone. There is decreased Tb.N and Conn.D in the *Trps1*^{col1a1} cKO females and males. Statistical significance is indicated by the asterisks beside the p-values: *-p ≤ 0.05, **p ≤ 0.01.

There are no statistical differences in the tissue mineral density of the alveolar bone in either males or females (Figure 18). These results tell us that the mineralization of trabecular bone within the alveolar bone is not affected in the *Trps1*^{col1a1} cKO mice when compared to the WT.

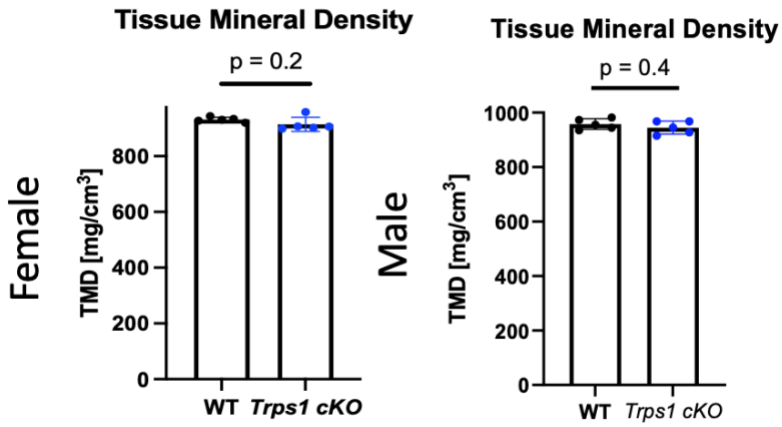

Figure 16: Comparison of WT and *Trps1*^{col1a1} cKO male and female tissue mineral density in the alveolar bone. There is no statistical significance.

The summary of the quantitative μCT analysis of the parameters that are statistically different between WT and *Trps1*^{col1a1} cKO mice is illustrated in Table 1. The females have more affected parameters for trabecular and cortical bone when compared to the males. However, both males and females had the same parameters affected in the *Trps1*^{col1a1} cKO when compared to the WT.

	Trabecular Bone	Cortical Bone	Alveolar Bone
Females	**Decreased:** • Trabecular Thickness • Total Volume • Bone Volume • Bone Volume Fraction • Tissue Mineral Density **Increased:** • Specific Bone Surface	**Decreased:** • Total Volume • Bone Volume • Bone Volume Fraction **Increased:** • Cortical Porosity	**Decreased:** • Total Volume • Bone Volume • Bone Volume Fraction • Trabecular Number • Connectivity Density
Males	**Decreased:** • Trabecular Thickness • Bone Volume **Increased:** • Specific Bone Surface	**Decreased:** • Total Volume	**Decreased:** • Total Volume • Bone Volume • Bone Volume Fraction • Trabecular Number • Connectivity Density

Table 1: Summary of the statistically significant parameters of the μCT quantitative analysis in the *Trps1*^{col1a1} cKO mice. The table shows the statistically significant parameters of the *Trps1*^{col1a1} cKO mice. There is a stronger phenotype in females for trabecular and cortical bone analysis. Created using Microsoft Word.

5.2 Osteoclast Analysis in *Trps1*^{col1a1} cKO Mice versus WT Mice

We wanted to determine the mechanism causing low bone mass in the *Trps1*^{col1a1} cKO mice. Histology and quantitative analysis of the left distal femurs of 4-week-old mice were used to determine if there were any differences in the osteoclasts between the WT and *Trps1*^{col1a1} cKO mice. This part of the project was a pilot study, so the minimum number needed for statistical analysis: n=3/genotype/sex were analyzed. Based off the observed difference between the WT and *Trps1*^{col1a1} cKO and the distribution of values within each group, we will estimate how many mice we must analyze to have more conclusive results. The parameters evaluated were osteoclast number per bone surface and osteoclast surface per bone surface. Gross microscopic evaluation of the chondro-osseous junction detected apparent stronger pink staining within the tissues and what appeared to be more osteoclasts stained throughout in the *Trps1*^{col1a1} cKO tissues when compared to the WT (Figure 20, A). Similarly, the 40x images taken at the trabecular bone regions showed what appears to be more pink staining within the trabecular bone and more osteoclasts throughout (Figure 20, B and C).

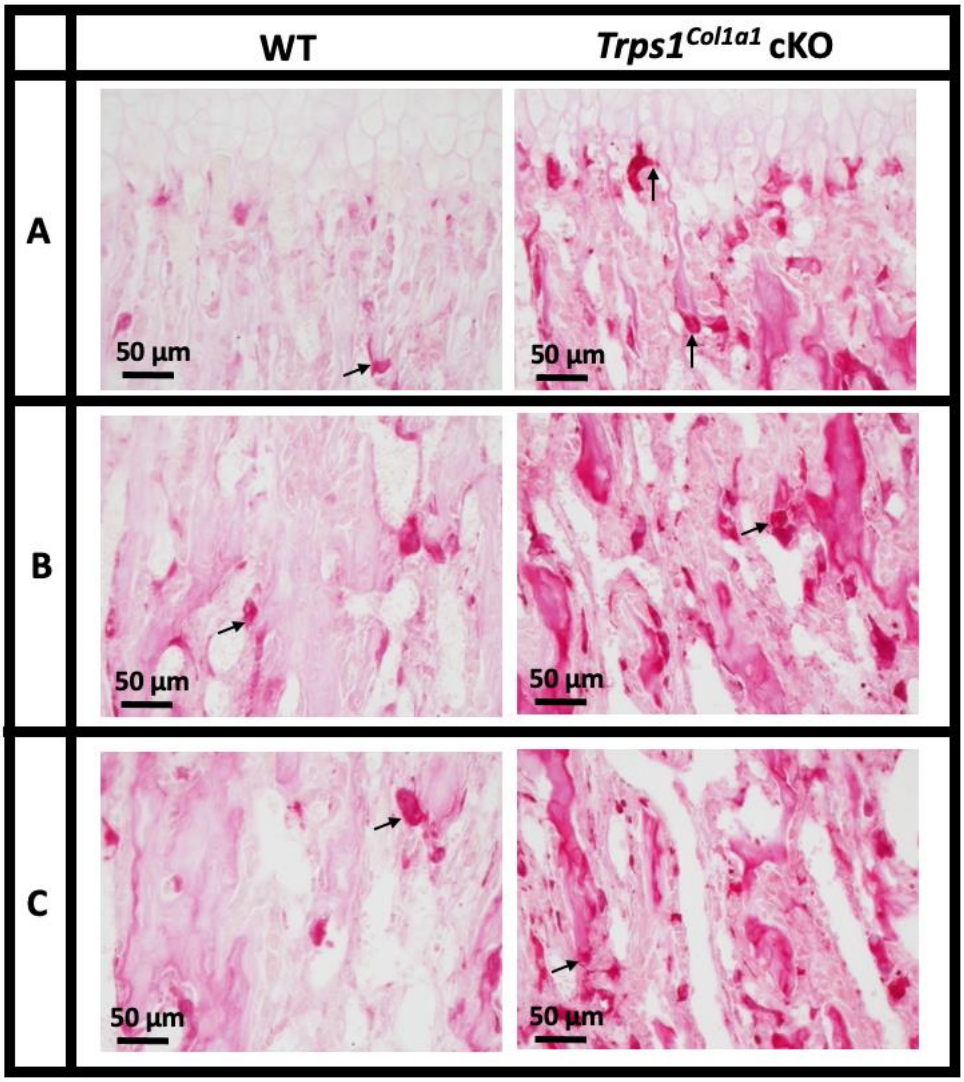

Figure 17: Comparison of WT and *Trps1*^{col1a1} cKO microscopic images at chondro-osseous junction and trabecular bone region to analyze osteoclast number. Osteoclasts indicated by arrows**.** Images taken at 40x magnification.

However, quantitative analysis of osteoclast surface per bone surface and osteoclast number per bone surface at the chondro-osseous junction detected no difference between WT and *Trps1*^{col1a1} cKO mice (Figure 21). Similarly, there was no statistically significant differences in osteoclast surface per bone surface and osteoclast number per bone surface for the trabecular bone analysis (Figure 22).

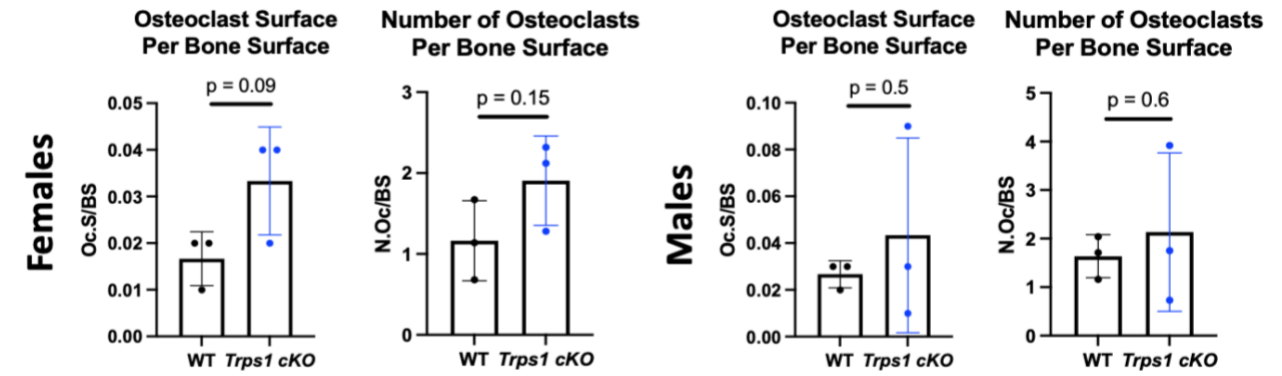

Figure 21: Quantitative analysis of WT and *Trps1*^{col1a1} cKO males and females osteoclast surface per bone surface and osteoclast number per bone surface at chondro-osseous junction. There is no statistical significance in the values.

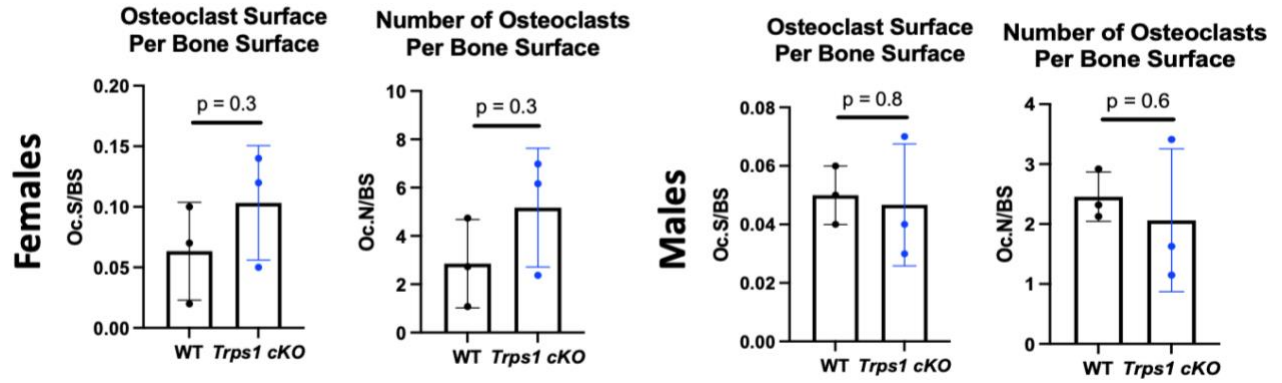

Figure 18: Quantitative analysis of WT and *Trps1*^{col1a1} cKO males and females osteoclast surface per bone surface and osteoclast number per bone surface on trabecular bone. There is no statistical significance in the values.

6.0 DISCUSSION AND LIMITATIONS

Bones constantly undergo remodeling to maintain bone microarchitecture, rearranging bone structure for enabling mechanical load, and for preserving systemic calcium homeostasis.[16] Bone remodeling is a process that occurs where old bone is resorbed by the bone resorbing cells called osteoclasts and new bone is formed by osteoblasts. The bone remodeling process is dependent on the tightly coupled communication between osteoclasts and osteoblasts. Age, certain medications, or genetic mutations cause a dysregulation in this balance between osteoclasts and osteoblasts, leading to too much bone resorption and not enough bone formation. This could be due to overactive osteoclasts or too many osteoclasts and not enough osteoblasts or impaired osteoblast function. This leads to low bone mass, called osteopenia or the more progressed form, osteoporosis.

Low bone mass impairs bone quality and leads to fracture susceptibility. One of the clinical characteristics of patients with TRPS is osteopenia or osteoporosis. We wanted to utilize a mouse model to mimic the clinical presentation of TRPS to have a better understanding of the role of *TRPS1* in bone development. We created a conditional knockout mouse model where *Trps1* is deleted specifically in osteoblasts upon tamoxifen injections. We utilized μCT to assess bone quantity and microarchitecture with quantitative analysis to compare the bone composition between WT and $Trps1^{col1a1}$ cKO male and female mice.

We found that the $Trps1^{col1a1}$ cKO mice have decreased trabecular bone in femurs and alveolar bone, with a stronger phenotype in females. There were no statistical differences in trabecular number or trabecular separation, but there appear to be two outliers in the $Trps1^{col1a1}$ cKO females which might be construing the data (Figure 9). The two outliers in the trabecular number graph are the same mice that are outliers in the graph representing the trabecular separation. This could mean that those two mice did not respond to the effects of the tamoxifen

injections; Cre may not have successfully been activated in those two mice.

There is decreased total volume, bone volume, and bone volume fraction, and increased cortical porosity in the *Trps1*^{col1a1} cKO females in the cortical bone, whereas males showed only a decrease in total volume. Male and female *Trps1*^{col1a1} cKO mice have less trabecular bone in the alveolar bone, and smaller alveolar bones. There is a decrease in trabecular number and connectivity density for alveolar bone in the *Trps1*^{col1a1} cKO when compared to the WT mice in both females and males (Figure 17). This indicates smaller trabeculae and suggests impaired bone quality; mechanical testing will need to be conducted to investigate bone quality.

The male and female *Trps1*^{col1a1} cKO have the same parameters affected in the alveolar bone analysis, but the females have more parameters affected in the femur and cortical bone analysis. The males do not have the same or as many parameters affected in the femur and cortical bone (Figure 19). This might indicate that *Trps1* deficiency in the osteoblasts may affect the females more in endochondral ossification when compared to intramembranous because the alveolar bone is formed through intramembranous ossification and the femur is formed through endochondral ossification.

For the osteoclast analysis, the images at 40x magnification showed that the TRAP staining was stronger in the *Trps1*^{col1a1} cKO mice when compared to the WT mice. However, quantitative analysis did not show any statistically significant differences between the WT and *Trps1*^{col1a1} cKO mice. The TRAP staining was a pilot experiment, in which we analyzed a minimum number of mice to be able to perform statistical analyses. With just n=3 mice/genotype, the graphs do show a trend of higher osteoclast surface per bone surface, and osteoclast number per bone surface in the *Trps1*^{col1a1} cKO female mice in comparison to the WT females. This suggests that analysis of more samples could reveal statistically significant differences.

Upon gross evaluation of the TRAP-stained tissue sections, *Trps1*^{col1a1} cKO trabecular

bones appear to have more TRAP activity as indicated by the intense pink color when compared to the WT mice. This could be because the trabeculae of *Trps1*^{col1a1} cKO mice are smaller and have more elaborated 3D structure, as revealed by our μCT analysis (Figure 7, 9, and 11). This 2D analysis may also not be as effective to analyze our 3D samples. An alternative would be to section the samples differently, where the sections are consecutively placed on a slide to analyze the depth of the femur to account for any osteoclasts that might have been segmented during the sectioning process. Consequently, the TRAP signal could be remnants of osteoclasts that if they were not segmented during the sectioning process, would have been visualized in their full size and darker pink color. Perhaps the osteoclasts that were anteriorly on the surface of the trabecular bone may have been segmented during the sectioning process and were not accounted for.

The BioQuant analysis was able to calculate osteoclast surface and osteoclast number normalized to the measured bone surface. We did not analyze the activity of osteoclasts. Thus, it could prospectively be that there are no differences in the number and surface of osteoclasts sitting on the trabecular surface of the 2D images analyzed, but that the osteoclasts were overactive in the *Trps1*^{col1a1} cKO mice. Another possibility could be that perhaps the impaired osteoblast function is why there is low bone mass in the WT and *Trps1*^{col1a1} *cKO* mice. Further analysis would need to be conducted to determine which mechanism is the reason for the low bone mass caused by *Trps1* deficiency in osteoblasts.

Possible future experiments could be to characterize osteoblasts. One way to do this would be to utilize fluorescence labeling with Calcein, which has high affinity to bone mineral to determine how much bone is actively being formed in vivo. In addition, we could investigate if there is impaired communication between the osteoblasts and osteoclasts through using an enzyme-linked immunosorbent assay (ELISA) to determine if there is any effect on the OPG/RANKL/RANK pathway. In vitro studies could also be utilized with *Trps1* KO osteoblasts in

order to determine their effect on osteoclast differentiation in a co-culture system.

7.0 CONCLUSIONS

Overall, we conclude that the *Trps1*^{col1a1} cKO mice are a good model for studying the mechanism of osteopenia in TRPS patients, as our μCT data showed smaller bone in the *Trps1*^{col1a1} cKO mice when compared to the WT male and female mice. In addition, our results suggest that there is sexual dimorphism, as there is a stronger phenotype in the *Trps1*^{col1a1} cKO females when compared to the males. Therefore, our results suggest that women with TRPS might be more susceptible to osteopenia than men. However, we would need to compare males to females to have conclusive results. Thus far, published studies of TRPS patients have not investigated whether women are more susceptible to osteopenia than men.

In addition to our μCT analysis, we would like to determine the mechanism causing the low bone mass in the TRPS patients. Visually, TRAP stain showed more stained osteoclasts in the *Trps1*^{col1a1} cKO mice when compared to the WT mice. However, our quantitative analysis did not show any statistically significant differences between the WT and *Trps1*^{col1a1} cKO mice. Further studies will be needed to determine if it is the osteoclasts that are causing too much resorption or if it is merely the osteoblasts that have impaired function.

Bibliography

1. Gai, Z., T. Gui, and Y. Muragaki, *The function of TRPS1 in the development and differentiation of bone, kidney, and hair follicles.* Histol Histopathol, 2011. **26**(7): p. 915-21.
2. Yang, L., et al., *Functional mechanisms of TRPS1 in disease progression and its potential role in personalized medicine.* Pathol Res Pract, 2022. **237**: p. 154022.
3. Malik, T.H., et al., *Transcriptional repression and developmental functions of the atypical vertebrate GATA protein TRPS1.* The EMBO Journal, 2001. **20**(7): p. 1715-1725.
4. Fantauzzo, K.A. and A.M. Christiano, *Trps1 activates a network of secreted Wnt inhibitors and transcription factors crucial to vibrissa follicle morphogenesis.* Development, 2012. **139**(1): p. 203-14.
5. Socorro, M., et al., *Deficiency of Mineralization-Regulating Transcription Factor Trps1 Compromises Quality of Dental Tissues and Increases Susceptibility to Dental Caries.* Front Dent Med, 2022. **3**.
6. Merjaneh, L., et al., *A novel TRPS1 gene mutation causing trichorhinophalangeal syndrome with growth hormone responsive short stature: a case report and review of the literature.* Int J Pediatr Endocrinol, 2014. **2014**(1): p. 16.
7. Maas, S., et al., *Trichorhinophalangeal Syndrome*, in *GeneReviews(®)*, M.P. Adam, et al., Editors. 1993, University of Washington, Seattle Copyright © 1993-2023, University of Washington, Seattle. GeneReviews is a registered trademark of the University of Washington, Seattle. All rights reserved.: Seattle (WA).
8. Trippella, G., et al., *An early diagnosis of trichorhinophalangeal syndrome type 1: a case report and a review of literature.* Ital J Pediatr, 2018. **44**(1): p. 138.
9. Breeland, G., M.A. Sinkler, and R.G. Menezes, *Embryology, Bone Ossification*, in *StatPearls*. 2023: Treasure Island (FL).
10. Yang, L., et al., *Hypertrophic chondrocytes can become osteoblasts and osteocytes in endochondral bone formation.* Proceedings of the National Academy of Sciences, 2014. **111**(33): p. 12097-12102.
11. St-Jacques, B., M. Hammerschmidt, and A.P. McMahon, *Indian hedgehog signaling regulates proliferation and differentiation of chondrocytes and is essential for bone formation.* Genes Dev, 1999. **13**(16): p. 2072-86.
12. Napierala, D., et al., *Uncoupling of chondrocyte differentiation and perichondrial mineralization underlies the skeletal dysplasia in tricho-rhino-phalangeal syndrome.* Human Molecular Genetics, 2008. **17**(14): p. 2244-2254.
13. Malik, T.H., et al., *Deletion of the GATA domain of TRPS1 causes an absence of facial hair and provides new insights into the bone disorder in inherited tricho-rhino-phalangeal syndromes.* Mol Cell Biol, 2002. **22**(24): p. 8592-600.
14. Kim, Y.J., et al., *Comprehensive Transcriptome Profiling of Balding and Non-Balding Scalps in Trichorhinophalangeal Syndrome Type I Patient.* Ann Dermatol, 2017. **29**(5): p. 597-601.
15. Socorro, M., et al., *Trps1 transcription factor represses phosphate-induced expression of SerpinB2 in osteogenic cells.* Bone, 2020. **141**: p. 115673.
16. Hadjidakis, D.J. and Androulakis, II, *Bone remodeling.* Ann N Y Acad Sci, 2006. **1092**: p. 385-96.

17. Weivoda, M.M., et al., *Identification of osteoclast-osteoblast coupling factors in humans reveals links between bone and energy metabolism.* Nat Commun, 2020. **11**(1): p. 87.
18. Chen, X., et al., *Osteoblast-osteoclast interactions.* Connect Tissue Res, 2018. **59**(2): p. 99-107.
19. Boyce, B.F. and L. Xing, *Functions of RANKL/RANK/OPG in bone modeling and remodeling.* Arch Biochem Biophys, 2008. **473**(2): p. 139-46.
20. Boyle, W.J., W.S. Simonet, and D.L. Lacey, *Osteoclast differentiation and activation.* Nature, 2003. **423**(6937): p. 337-342.
21. Cho, K.Y., et al., *Trps1 Regulates Development of Craniofacial Skeleton and Is Required for the Initiation of Palatal Shelves Fusion.* Front Physiol, 2019. **10**: p. 513.
22. Kim, J.E., K. Nakashima, and B. de Crombrugghe, *Transgenic mice expressing a ligand-inducible cre recombinase in osteoblasts and odontoblasts: a new tool to examine physiology and disease of postnatal bone and tooth.* Am J Pathol, 2004. **165**(6): p. 1875-82.
23. Starnes, L.M., et al., *Increased bone mass in male and female mice following tamoxifen administration.* Genesis, 2007. **45**(4): p. 229-35.
24. Wang, L., et al., *Trps1 differentially modulates the bone mineral density between male and female mice and its polymorphism associates with BMD differently between women and men.* PLoS One, 2014. **9**(1): p. e84485.
25. Gj, A., et al., *Microarchitecture and morphology of bone tissue over a wide range of BV/TV assessed by micro-computed tomography and three different threshold backgrounds.* Med Eng Phys, 2022. **106**: p. 103828.